

X-RAY FLARES FROM MARKARIAN 501

Yongquan Xue and Wei Cui

Department of Physics, Purdue University, West Lafayette, IN 47907;
xuey@physics.purdue.edu, cui@physics.purdue.edu

ABSTRACT

Motivated by the recent finding of hierarchical X-ray flaring phenomenon in Mrk 421, we conducted a systematic search for X-ray flares from Mrk 501, another well-known TeV blazar, by making use of the rich *RXTE* archival database. We detected flares over a wide range of timescales, from months down to minutes, as in the case of Mrk 421. However, the flares do not seem to occur nearly as frequently in Mrk 501 as in Mrk 421 on any of the timescales. The flaring hierarchy also seems apparent in Mrk 501, suggesting that it might be common among TeV blazars. The results seem to imply a scale-invariant physical origin of the flares (large or small). The X-ray spectrum of the source shows a general trend of hardening toward the peak of long-duration flares, with indication of spectral hysteresis, which is often seen in TeV blazars. However, the data are not of sufficient quality to allow us to draw definitive conclusions about spectral variability associated with more rapid but weaker flares. We critically examine a reported sub-hour X-ray flare from Mrk 501, in light of intense background flaring activity at the time of the observation, and concluded that the flare is likely an artifact. On the other hand, we did identify a rapid X-ray flare that appears to be real. It lasted only for about 15 minutes, during which the flux of the source varied by about 30%. Sub-structures are apparent in its profile, implying variabilities on even shorter timescales. Such rapid variabilities of Mrk 501 place severe constraints on the physical properties of the flaring region in the jet, which have serious implications on the emission models proposed for TeV blazars.

Subject headings: BL Lacertae objects: individual (Markarian 501) — galaxies: active — radiation mechanisms: non-thermal — X-rays: galaxies

1. Introduction

Mrk 501 is among the brightest and closest ($z = 0.034$) extragalactic X-ray sources in the sky. It is classified as a BL Lacertae object and is located in the elliptical galaxy UGC

10599 (Stickel et al. 1993). BL Lac objects belong to a more general class of radio-loud active galactic nuclei known as blazars, which are characterized by rapid variability and non-thermal emission at nearly all wavelengths. The emission from a blazar is generally thought to be dominated by radiation from a relativistic jet that is directed roughly along the line of sight (Urry & Padovani 1995). The spectral energy distribution (SED) of blazars invariably shows two characteristic “humps” in the νF_ν representation, with one located at optical–X-ray energies and the other at GeV–TeV energies (Fossati et al. 1998). Mrk 501 is among a small number of blazars that have been detected at TeV energies (e.g., Quinn et al. 1996; Bradbury et al. 1997).

For TeV blazars, there is a general correlation between fluxes at X-ray and TeV energies (where the SED peaks), although exceptions have recently been noted (Krawczynski et al. 2004; Cui et al. 2004). While the origin of gamma rays is still being debated, there is a general consensus that X-rays originate in the synchrotron radiation from highly relativistic electrons in the jet. Two classes of models have been proposed to explain gamma-ray emission from blazars. In the leptonic models, the TeV emission is attributed to the synchrotron self-Compton (SSC) process (e.g., Marscher & Gear 1985; Maraschi et al. 1992). The SSC models are attractive for their conceptual simplicity. They can quite naturally account for the observed X-ray–TeV correlation, and have also enjoyed some success in fitting the observed SEDs (e.g., Kataoka et al. 1999; Sambruna et al. 2000; Petry et al. 2000; Krawczynski et al. 2002; Konopelko et al. 2003). However, such models still face challenges, such as the presence of “orphan TeV flares” (i.e., those TeV flares with no apparent counterparts in X-rays; Krawczynski et al. 2004; Cui et al. 2004). In the hadronic models, the TeV emission is probably due to synchrotron radiation from relativistic protons in the jet (Aharonian 2000; Mücke et al. 2003), although other hadronic processes might also contribute. Although the models are being pushed to the limit by the observed rapid variability of TeV blazars, they are, by no means, ruled out yet. It remains to be seen whether they can account for the X-ray–TeV correlation in a quantitative manner.

TeV blazars are known to undergo flaring activities both at X-ray and TeV energies. The flares seem to occur on all timescales but vary greatly in magnitude, as illustrated vividly by the X-ray flaring hierarchy in Mrk 421 (Cui 2004). The hierarchy strongly implies the scale-invariant nature of flaring processes in the source, prompting comparison to solar flares and seemingly similar rapid flares in stellar-mass black hole systems. The flares from Mrk 501 have been well observed at X-ray and TeV energies (e.g., Quinn et al. 1996; Bradbury et al. 1997; Catanese et al. 1997; Hayashida et al. 1998; Kataoka et al. 1999; Sambruna et al. 2000; Petry et al. 2000). In fact, the detection of a very rapid X-ray flare from the source was reported (Catanese & Sambruna 2000), which represented the first case of sub-hour X-ray flares in any TeV blazar. The short duration of the flare would lead to severe constraints on

the properties of the flaring region, as in the case of Mrk 421 (Cui 2004).

Motivated by the recent finding of hierarchical X-ray flaring phenomenon in Mrk 421 (Cui 2004), we conducted a systematic search for X-ray flares in Mrk 501 over a broad range of timescales, making use of the rich *RXTE* archival database. We describe the data and data reduction procedure in § 2. The results are presented in § 3, along with a critical examination of the reported sub-hour X-ray flare. Finally, in § 4, we discuss the results and their implications on the proposed models.

2. Data and Data Reduction

Mrk 501 has been observed frequently with *RXTE*. For this work, we obtained publicly available data from the archival databases, including data both from the All-Sky Monitor (ASM) and the Proportional Counter Array (PCA). We obtained the ASM light curves of Mrk 501 from the MIT archive.¹ We chose to filter out data points with error bars (on the raw count rates in the summed band) greater than 2.0 counts/s, which constitute about 5% of the data. We then weighted the rates by $1/\sigma^2$ and rebinned them to produce light curves with 21-day time bins. The light curves are available in three energy bands: 1.5–3, 3–5, and 5–12 keV, providing crude spectral information.

The PCA is a narrow-field, pointing instrument. It consists of five nearly identical proportional counter units (PCUs) and covers a nominal energy range of 2–60 keV. Due to operational constraints, some of the PCUs were often switched off. Only PCU 0 and PCU 2 are nearly always in operation. Data analysis is further complicated by the loss of the front veto layer in PCU 0 (in 2000), because the data from PCU 0 is now more prone to contamination by events caused by low-energy electrons entering the detector. This is particularly relevant to the study of variability of weak sources like Mrk 501. Fortunately, it only affects a about 15% of the data used in this work. We excluded from timing analyses PCU 0 data collected in 2000. Most PCA observations were made in “snap-shot” modes, with typical effective exposure times ranging from half a kilosecond to a few kiloseconds. The PCA has numerous data modes and multiple modes are usually employed in an observation. For this work, however, we only used the *Standard 2* data, which have a time resolution of 16 s.

We followed Cui (2004) closely in reducing and analyzing the PCA data. Briefly, the data were reduced with *FTOOLS 5.2*. For an observation, we first filtered data by fol-

¹See <http://xte.mit.edu/asmlc/srcs/mkn501.html#data>

lowing the standard procedure for faint sources (see the online *RXTE* Cook Book),² which resulted in a list of good time intervals (GTIs). We then simulated background events for the observation with the latest background model that is appropriate for faint sources (`pca_bkgd_cmfaint17_eMv20031123.mdl`). Using the GTIs, we proceeded to extract a light curve from the data (by combining all active PCUs) in each of the following energy bands: 2.0–5.7, 5.7–11, 11–60, and 2.0–60 keV. Note that the boundaries of each band are matched up as closely as possible across different PCA epochs but are only approximate (up to ± 0.2 keV). We repeated the steps to construct the corresponding background light curves from the simulated events. Finally, we obtained light curves of the source by subtracting off the background. Following a similar procedure, we constructed an X-ray spectrum and the associated background spectrum for each observation. We note that for spectral analysis we only used data from the first xenon layer of each PCU (which is most accurately calibrated). For the purpose of detailed spectral modeling (see § 3.4), we included a 1% systematic uncertainty uniformly across the entire energy range of interest, to take into account residual calibration uncertainties. Note that we did include PCU 0 data from the 2000 observations in the spectral analysis because the background model for the detector seems to work fine in all cases.

3. Results

3.1. Long X-ray Flares: Months to > Year

Figure 1 shows the ASM light curve of Mrk 501 for the 1.5–12 keV band over roughly an eight-year period. The source was very active in X-rays in 1997. The activity continued, at a much lower level, in 1998 and also the early part of 1999. Mrk 501 has been relatively quiet ever since. At least two major flares are easily identifiable from the light curve, which lasted for months to over a year. The flares show substantial sub-structures, indicating variability on shorter timescales, perhaps in the form of unresolved weaker and shorter flares.

Though crude, hardness ratios make it possible to study, in a model-independent manner, spectral variability of a source. Here, we computed the ratio between the ASM count rate in the 3–12 keV band to that in the 1.5–3 keV band to examine spectral evolution of Mrk 501 during the 1997 giant flare. The results are shown in Figure 2. For clarity, we have averaged the raw ASM count rates with variable time bins (6-week, 2-week, and 1-week), depending on the brightness of the source. The figure clearly shows a hardening trend of

²See http://heasarc.gsfc.nasa.gov/docs/xte/recipes/cook_book.html.

the X-ray spectrum as the source approaches the peak of the flare. This is consistent with findings of previous works (e.g., Pian et al. 1998). Such a hardness-intensity correlation seems to hold in general for X-ray bright blazars (Giommi et al. 1990).

To investigate the phenomenon of spectral hysteresis, which is often observed in blazars (e.g., Takahashi et al. 1996, Kataoka et al. 2000, Zhang 2002, Giebels et al. 2002, Falcone et al. 2004, Cui 2004) but may be too subtle to be seen in the ASM data, we made a similar hardness-intensity diagram from the PCA data. There are three observing periods, with two covering the rising portion of the 1997 flare and one the decaying portion, as shown in Figure 3 (top panel). Unfortunately, the coverage of the flare with the PCA is quite sparse, especially during the decaying phase. While there appears to be indication of spectral hysteresis during the rising phase (perhaps associated with smaller flares) and between the rising and decaying phases, it is difficult to draw any definitive conclusions from these results. On the other hand, the trend of spectral hardening with increasing fluxes is also apparent in the PCA data.

3.2. Intermediate X-ray Flares: Days to Weeks

The PCA data span a period of 4 years, which covers weaker flaring activities in 1998, 1999, and 2000, besides the giant flare in 1997 (see Fig. 1). The light curves reveal the presence of X-ray flares with shorter durations, from days to weeks, nearly all the time, as shown in Figure 4. Although the ASM light curve shows that the source seems to be very quiet during the PCA observations in 1999 and 2000, the more sensitive PCA light curves reveal flaring activities during these time periods. Therefore, like Mrk 421, there is no apparent “quiescent” state for Mrk 501 either. Unlike Mrk 421, however, the flux of Mrk 501 does not seem to vanish, implying the presence of steady-state emission. The amplitude of these intermediate flares can also be very large, up to 4–5 times the steady-state flux. We attempted to investigate spectral evolution and hysteresis of the source across individual flares but found that the results were ambiguous, mainly due to the lack of quality of the data in this case.

3.3. Rapid X-ray Flares: < Hour

Catanese & Sambruna (2000) reported the first case of a sub-hour X-ray flare from Mrk 501. Surprisingly, however, we initially failed to find it in the PCA light curves constructed from the same observation. Examining the light curves more carefully, we realized that

there was actually a data gap almost exactly at the time of the flare. We suspected that the data had probably been filtered out during the data cleaning process in our case. We then relaxed the data filtering criteria one at a time and in the end found that it was the high “ELECTRON2” values that deemed the time interval (of the reported flare) “bad”. In general, the “ELECTRON” parameter provides a measure of contamination of the data by events induced by electrons entering the detector. Some of such events (due to low energy electrons) may be registered as good X-ray events because they fail to trigger any of the vetoing logics. Since the PCU 2 is always on, we used “ELECTRON2” in the data cleaning procedure (as recommended in the *RXTE* Cookbook).

To show possible electron contamination of the data, we plotted the X-ray count rates and the values of the “ELECTRON2” parameter for the observation in Figure 5 (left panels). The figure clearly shows that there is a strong electron flare nearly at the same time as the reported X-ray flare, which raises the possibility of the latter being an artifact. However, we note that the X-ray flare seems to have started about 200 s before the electron flare and that the profile of the X-ray flare appears asymmetric, unlike that of the electron flare. We cannot think of an obvious explanation for either “anomaly”. On the other hand, we found another rapid X-ray flare (which has not been reported) from a different observation (obsid: 30249-01-01-01), which also has an asymmetric profile, is accompanied by an electron flare, and leads the electron flare by about the same amount of time (~ 200 s), as also shown in Fig. 5 (right panels) for a direct comparison. The presence of two such flares raised serious doubts in our mind about them being physically associated with Mrk 501.

We then systematically searched for X-ray flares that were accompanied by electron flares, by visually inspecting all of the light curves, and found a total of 21 cases (although it is entirely possible that some weaker ones might have escaped our attention), including the two just discussed. Interestingly, in all other 19 cases, we found no apparent timing offsets between X-ray and electron flares. Figure 6 shows some representative examples of those. It is clear, from the figure, that not all electron flares are registered as X-ray signals and that the profile of an electron flare can be complex, e.g., with multiple peaks. Moreover, we found that the spectrum of the X-ray flares varies greatly. In extreme cases, a single X-ray flare is seen in one energy band that coincides with one of the peaks of an electron flare, but another flare in a different energy band that coincides with a different peak of the same electron flare. Therefore, the phenomenology is complex.

Finally, we derived the latitude and longitude of the *RXTE* satellite at the time of the peak of each of the 21 electron flares. Figure 7 shows a map that summarizes the results. The two cases shown in Fig. 5 are highlighted with different symbols. It should be noted that the peaks of these two electron flares are separated by almost exactly one satellite orbit

(≈ 1.6 hours). In general, the electron flares seem to cluster in the northeast Pacific region, which confirms what is generally known about the occurrence of such events (K. Jahoda and C. Markwardt of the PCA team, private communication). However, particle fluxes in the region are usually over two orders of magnitude smaller than those in the well-known South Atlantic Anomaly (SAA) region, which is why the region is not screened in the same manner as the SAA. Putting together all the evidences, we think that the reported rapid flare (and also the one found in this work) is most likely an artifact caused by intense flaring in soft electron fluxes. Admittedly, outstanding issues remain regarding the observed timing offsets or asymmetric profiles (see Fig. 5). Neither can we rule out the possibility that real flares from Mrk 501 might sometimes include a very soft second delayed component, which increases the “ELECTRON” parameter through extra counts absorbed in the propane layer, although the scenario seems a bit contrived.

In our search, we discovered yet another sub-hour X-ray flare. It occurred during an observation (obsid: 30249-01-01-02) when there was hardly any enhancement in the soft electron fluxes. Figure 8 shows the flare, along with the “ELECTRON2” parameter for the same time period. The flare is quite weak (compared with the other two), reaching a peak amplitude of about 30% of the steady-state flux. It lasted for about 800 s and shows sub-structures on even shorter timescales. The profile shown might represent the composite of two flares or a sudden decrease and recovery of X-ray fluxes in the middle of a flare. Remarkably, the rising or decaying time associated with the sub-structures is as short as about 20–30 seconds! The flare occurred roughly one satellite orbit after the reported one, which might be a bit worrisome. However, it would appear about 50° in longitude further west (as shown in Fig. 7). Moreover, Mrk 501 was monitored very intensely during this time period, with data taken in 18 nearly consecutive satellite orbits. Most of these observations did indeed span periods when the satellite was in the general area of the “Northeast Pacific Region”, but no X-ray/electron flare (other than the ones already mentioned) was detected, which rules out any systematic effects associated with the region. Finally, if the flare shown in Fig. 8 were to be false, it would have to be caused by a surge in particle-induced events that were not vetoed *and* not manifested in the increase of the “ELECTRON” factor; we are not aware of any examples of such background flaring activities. Therefore, we believe that we have detected a sub-hour flare from Mrk 501. The rare detection can be attributed, to a large extent, to the much intensified coverage of the source.

3.4. Spectral Modeling

We carried out detailed spectral modeling to investigate, in a more quantitative manner, spectral variability of Mrk 501. Here, we eliminated all observations with effective exposure times less than 200 s, because of the lack of statistics. In subsequent analyses, we fixed the hydrogen column density at $1.8 \times 10^{20} \text{ cm}^{-2}$ (Dickey & Lockman 1990). We experimented with the following empirical models: power law, power law with an exponential rollover, and broken power law, to fit the observed X-ray spectra. We found that when the source was relatively weak (the 2–20 keV flux less than $2 \times 10^{-10} \text{ ergs cm}^{-2} \text{ s}^{-1}$), the power-law model fits the X-ray spectra well. However, the simple model fails statistically (in terms of χ^2 values) at higher fluxes. The data taken when the source was brighter (in 1997 and parts of 1998) clearly favor the broken power-law model. Formally, the resultant fits are satisfactory (with the reduced χ^2 values all around unity).

Mrk 501 was most active in 1997, with the 2–20 keV flux varying roughly between $3\text{--}9.5 \times 10^{-10} \text{ ergs cm}^{-2} \text{ s}^{-1}$. The best-fit broken power-law parameters are summarized in Figure 9. The first photon index shows an initial decreasing (or spectral hardening) trend and then levels off toward high fluxes; so does the second photon index, although the trend is less apparent. In general, the SED of Mrk 501 is quite flat in the X-ray band during this time period. Spectral variability seems to be dominated by changes in the break energy (roughly between 5 and 16 keV). In the subsequent years (1998–2000), the source became much weaker in X-rays, with the flux ranging between $0.4\text{--}4 \times 10^{-10} \text{ ergs cm}^{-2} \text{ s}^{-1}$. The broken power-law model is still required for some of the 1998 observations, as already mentioned, and the results are also shown in Fig. 9 for comparison. The photon indices show large variations. In some cases, the X-ray spectrum is significantly steeper than that observed in 1997. On the other hand, the values of the break energy seem comparable to those from the 1997 observations.

At lower fluxes ($< 2 \times 10^{-10} \text{ ergs cm}^{-2} \text{ s}^{-1}$), the data can no longer effectively constrain the broken power-law model, mainly due to the lack of statistics (and also to the fact that the photon indices above and below the break do not differ significantly; see Fig. 9). Figure 10 shows the results from fits with a simple power law. The trend of spectral hardening toward high fluxes is more apparent in this case. The photon index goes roughly from 2.6 down to 1.8, clearly indicating a shift in the synchrotron SED peak toward higher energies at higher fluxes. Also apparent from the figure is spectral hysteresis associated with the 1998 observations. As shown in Fig. 1, these observations sampled two distinct periods: the very end of the decaying phase of the 1997 giant flare and the rising phase of a subsequent major flare (of much lower magnitude). To examine spectral hysteresis in more detail, we marked the data points with different symbols for the two periods in Figures 9 and 10. For

the most part, the points seem to bifurcate, with those for each period clustered around one of the branches. However, the phenomenon is clearly more complex — spectral hysteresis also seems to be present within each period, perhaps associated with smaller flares that are not resolved.

4. Discussion

Like Mrk 421, Mrk 501 also produces X-ray flares on a wide range of timescales. Unlike in Mrk 421, however, the flares in Mrk 501 do not seem to occur nearly as frequently, which appears to be the case on all timescales. This would be consistent with the scale invariance of X-ray flaring phenomenon, if it is common among TeV blazars. Fig. 11 illustrates the flaring hierarchy observed in Mrk 501. In other words, there might not be any fundamental differences among long flares, intermediate flares, or rapid flares, because they could all be caused by the same physical process operating on all physical scales. Though not fully understood, the flares in blazars are often thought to be related to internal shocks in the jet (e.g., Rees 1978; Spada et al. 2001), or to major ejection events of new components of relativistic plasma into the jet (e.g., Böttcher et al. 1997; Mastichiadis & Kirk 1997). In these scenarios, the flares of different durations might simply be the observational manifestation of a hierarchy of inhomogeneities in the jet, which are energized to produce flares by the shocks. Alternatively, the flares might be associated with magnetic reconnection events in a magnetically dominated jet (Lyutikov 2003), perhaps similar to solar flares in this regard. The flaring hierarchy might be related to reconnection and subsequent avalanche processes. We should note that the proton-synchrotron model actually requires a magnetically dominated jet to account for the observed TeV emission from blazars (Aharonian 2000; Mücke et al. 2003).

The X-ray spectrum of Mrk 501 evolved significantly during the 1997 and 1998 major flares. It shows a general trend of hardening toward the peak of a flare, which is consistent with results from previous works on X-ray bright blazars (Giommi et al. 1990), perhaps implying a hardening in the spectral distribution of the emitting electrons during the major flares. Moreover, there are indications of hysteresis associated with the spectral evolution of the source during major flares in 1997 and 1998. Though common among blazars, spectral hysteresis is still not fully understood. Kirk & Mastichiadis (1999) showed, using an internal shock model, that complex hysteresis behavior could arise from the interplay of three characteristic timescales associated with synchrotron cooling (τ_{syn}), particle acceleration (τ_{acc}), and intrinsic variability (τ_{var}), respectively. The model can qualitatively describe the observed spectral hysteresis associated with rapid flares, but would have difficulty in explaining the

phenomenon associated with long-duration flares in Mrk 501, because τ_{var} almost certainly dominate over τ_{syn} and τ_{acc} in the latter cases.

We critically examined the reported sub-hour X-ray flare from Mrk 501 (Catanese & Sambruna 2000), in light of intense background flaring activities during the observation. We found that it was likely associated with flaring activities in the flux of soft electrons entering the detectors, as opposed to those of Mrk 501. A similar rapid X-ray flare was detected in this work, which was also accompanied with a strong electron flare. On the other hand, we also found a rapid X-ray flare that occurred during a time that seems to be free of any background flaring activities. The flare lasted only for about 800 s; it might in fact be composed of two flares on even shorter timescales. These variability timescales pose severe constraints on the physical properties of the flaring region. First of all, the (jet-frame) size of the region is constrained by $l \lesssim ct_{flare}\delta/(1+z) = 2.4 \times 10^{14}\delta_1 \text{ cm}$, where t_{flare} is the duration of the flare ($= 800 \text{ s}$), δ is the Doppler factor of the jet ($\delta = 10\delta_1$), and z is the redshift of Mrk 501 ($= 0.034$). The upper limit is already comparable to the gravitational radius ($r_g \equiv GM/c^2$) for a $1.3 \times 10^9 M_\odot$ black hole, which is believed to exist in Mrk 501 (Barth et al. 2003), if the Doppler factor of the jet is not too much larger than 10 (which is probably the case; see discussion below). Since the peak flux of the flare is a significant fraction of the steady-state flux, the size of the flaring region is probably comparable to the lateral extent of the jet. If the jet originates from accretion flows, as is often thought to be the case, the result would also represent an upper limit on inner boundary of the flows (either in the form of a geometrically thin, optically thick cold disk or of a geometrically thick, optically thin hot torus).

Secondly, the observed decaying time of the flare sets a firm upper limit on the synchrotron cooling time of the emitting electrons. The cooling time is given by Rybicki & Lightman (1979), $\tau_{syn} \approx 6\pi m_e c / \sigma_T \gamma_p B^2$, where m_e is the electron rest mass, σ_T is the Thomson cross section, B is the strength of the magnetic field in the region, and γ_p is the characteristic Lorentz factor of those electrons that contribute to the bulk of the observed X-ray emission (at $E_p \sim 10 \text{ keV}$, where the synchrotron peak of the SED lies). From $\tau_{syn}/\delta < t_d$, where t_d is the decaying time of the flare ($\approx 400 \text{ s}$), we can derive a lower limit on the magnetic field strength, $B > 1.4\delta_1^{-1/2}\gamma_{p,5}^{-1/2} G$, where $\gamma_p = 10^5\gamma_{p,5}$. This is already larger than typical values of B inferred from fitting the SED with the SSC models (e.g., Kataoka et al. 1999; Sambruna et al. 2000; Petry et al. 2000; Krawczynski et al. 2002; Konopelko et al. 2003). Finally, for synchrotron photons to reach X-ray energies (at $\sim E_p$), the Lorentz factor of the emitting electrons must be sufficiently high, $E_p = \delta h\nu_c \equiv (3eh/4\pi m_e c)\delta\gamma_p^2 B$ (Rybicki & Lightman 1979). Using the derived lower limit on B , we can derive an *upper* limit on the Doppler factor, $\delta < 6.4E_{p,1}^2(\gamma_{p,5}/3)^{-3}$, which seems quite low compared to typical values inferred from the SSC models.

We thank Keith Jahoda and Craig Markwardt for insightful discussions on the issue of electron contamination and the referee for his/her very detailed and constructive comments. This work was supported in part by grants from the US Department of Energy and National Aeronautics and Space Administration. We made use of data obtained through the High Energy Astrophysics Science Archive Research Center Online Service, provided by the NASA/Goddard Space Flight Center.

REFERENCES

- Aharonian, F. 2000, *New Astronomy*, 5, 377
- Barth, A. J., Ho, L. C., & Sargent, W. L. W. 2003, *ApJ*, 583, 134
- Böttcher, M., et al. 1997, *A&A*, 324, 395
- Bradbury, S., et al. 1997, *A&A*, 320, L5
- Catanese, M., et al. 1997, *ApJ*, 487, L143
- Catanese, M., & Sambruna, R. M. 2000, *ApJ*, 534, L39
- Cui, W. 2004, *ApJ*, 605, 662
- Cui, W., et al. 2004, Proc. "International Symposium on High Energy Gamma-Ray Astronomy" (Gamma-2004, Heidelberg, Germany), eds. F. A. Aharonian and H. Voelk, AIP Proceedings Series (astro-ph/0410160)
- Dickey & Lockman, 1990, *ARAA*, 28, 215
- Falcone, A. D., Cui, W., & Finley, J. P. 2004, *ApJ*, 601, 165
- Fossati, G., Maraschi, L., Celotti, A., Comastri, A. & Ghisellini, G. 1998, *MNRAS*, 299, 433
- Giebels, B., et al. 2002, *ApJ*, 571, 763
- Giommi, P., Barr, P., Pollock, A. M. T., Garilli, B., & Maccagni, D. 1990, *ApJ*, 356, 432
- Hayashida, N., et al. 1998, *ApJ*, 504, L71
- Kataoka, J., et al. 1999, *ApJ*, 514, 138
- Kataoka, J., et al. 2000, *ApJ*, 528, 243
- Kirk, J. G. & Mastichiadis, A. 1999, *Astropart. Phys.*, 11, 45
- Konopelko, A., Mastichiadis, A., Kirk, J., de Jager, O. C., & Stecker, F. W. 2003, *ApJ*, 597, 851
- Krawczynski, H., Coppi, P. S., & Aharonian, F. 2002, *MNRAS*, 336, 721

- Krawczynski, H., et al. 2004, *ApJ*, 601, 151
- Lyutikov, M. 2003, *New Astr. Rev.* 47, 513
- Maraschi, L., Ghisellini, G., & Celotti, A., 1992, *ApJ*, 397, L5
- Marscher, A. P., & Gear, W. K., 1985, *ApJ*, 298, 114
- Mastichiadis, A., & Kirk, J. G. 1997, *A&A*, 320, 19
- Mücke, A., Protheroe, R.J., Engel, R., Rachen, J. P., & Stanev, T. 2003, *APh*, 18, 593
- Petry, D., et al. 2000, *ApJ*, 536, 742
- Pian, E., et al. 1998, *ApJ*, 492, L17
- Quinn, J., et al. 1996, *ApJ*, 456, L83
- Rees, M. J. 1978, *MNRAS*, 184, P61
- Rybicki, G. B., & Lightman, A. P., *Radiative Processes in Astrophysics* (New York: John Wiley & Sons)
- Sambruna, R. M., et al. 2000, *ApJ*, 538, 127
- Spada, M., et al. 2001, *MNRAS*, 325, 1559
- Stickel, M., Fried, J. W., & Kuehr, H. 1993, *A&AS*, 98, 393
- Takahashi, T., et al. 1996, *ApJ*, 470, L89
- Urry, C. M., & Padovani, P. 1995, *PASP*, 107, 803
- Zhang, Y, H. 2002, *MNRAS*, 337, 609

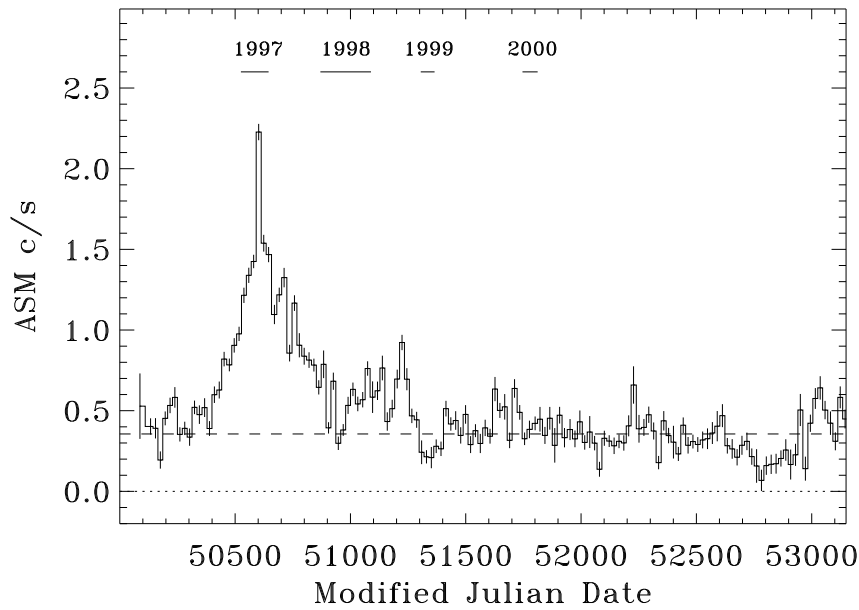


Fig. 1.— ASM light curve of Mrk 501. Each data point was derived from a weighted average of raw count rates over 21 consecutive days (after filtering out the “bad data”; see text). The error bars shown represent the standard deviations. The dashed-line roughly shows the average count rate of the source in the “low state” (which is an average of the rates between MJD 51400–53150). The periods of monitoring campaigns (with the pointing instruments) are indicated.

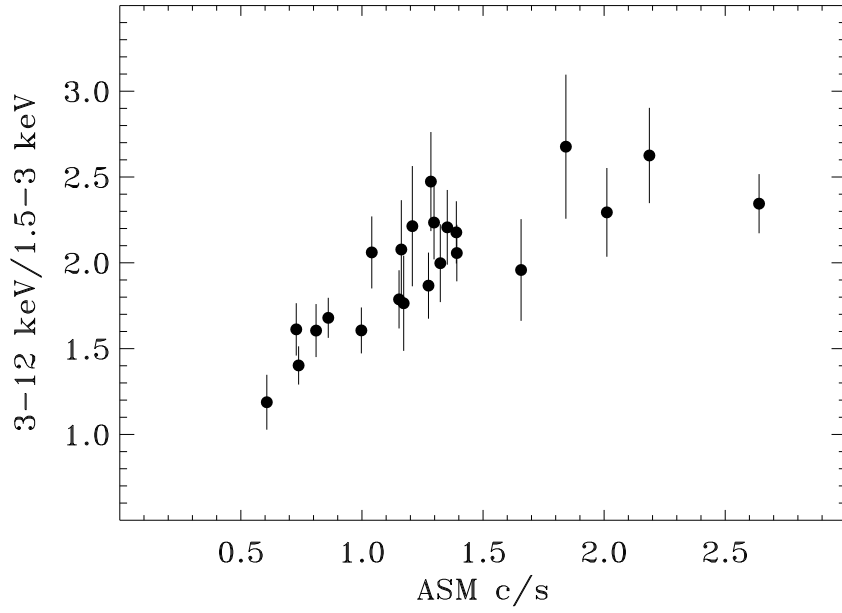


Fig. 2.— ASM hardness-intensity diagram for the 1997 giant flare (MJD 50442–50875). Note a general hardening trend of the X-ray spectrum as the flux increases.

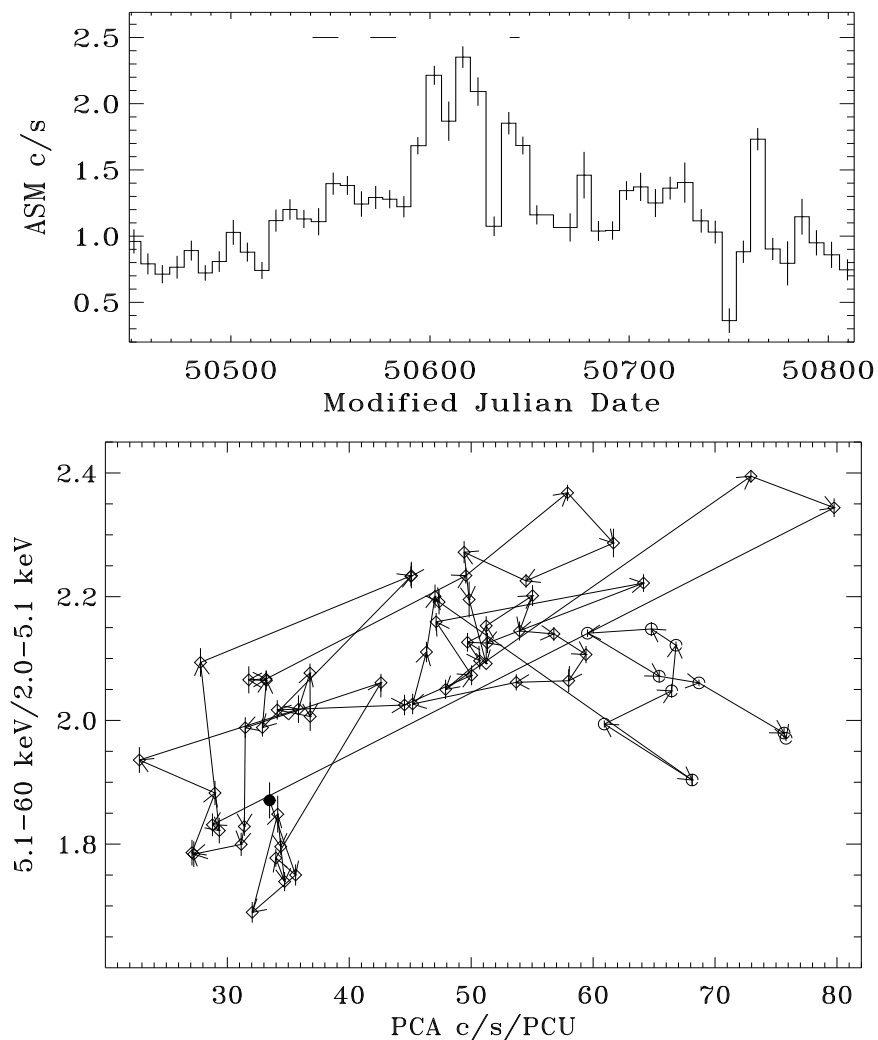


Fig. 3.— (top) Expanded ASM view of the 1997 giant flare. The count rates are weekly averaged in this case. The horizontal lines at the top indicate periods of the PCA observations. (bottom) PCA hardness-intensity diagram. The count rates were computed for the 2–60 keV band. Data taken during the rising portion of the flare are shown in open diamonds (except for the very first data point, which is indicated by a filled circle), while data during the decaying phase in open circles. The direction of the arrows shows the time progression of the flare. Note the general trend of spectral hardening toward the peak of the flare.

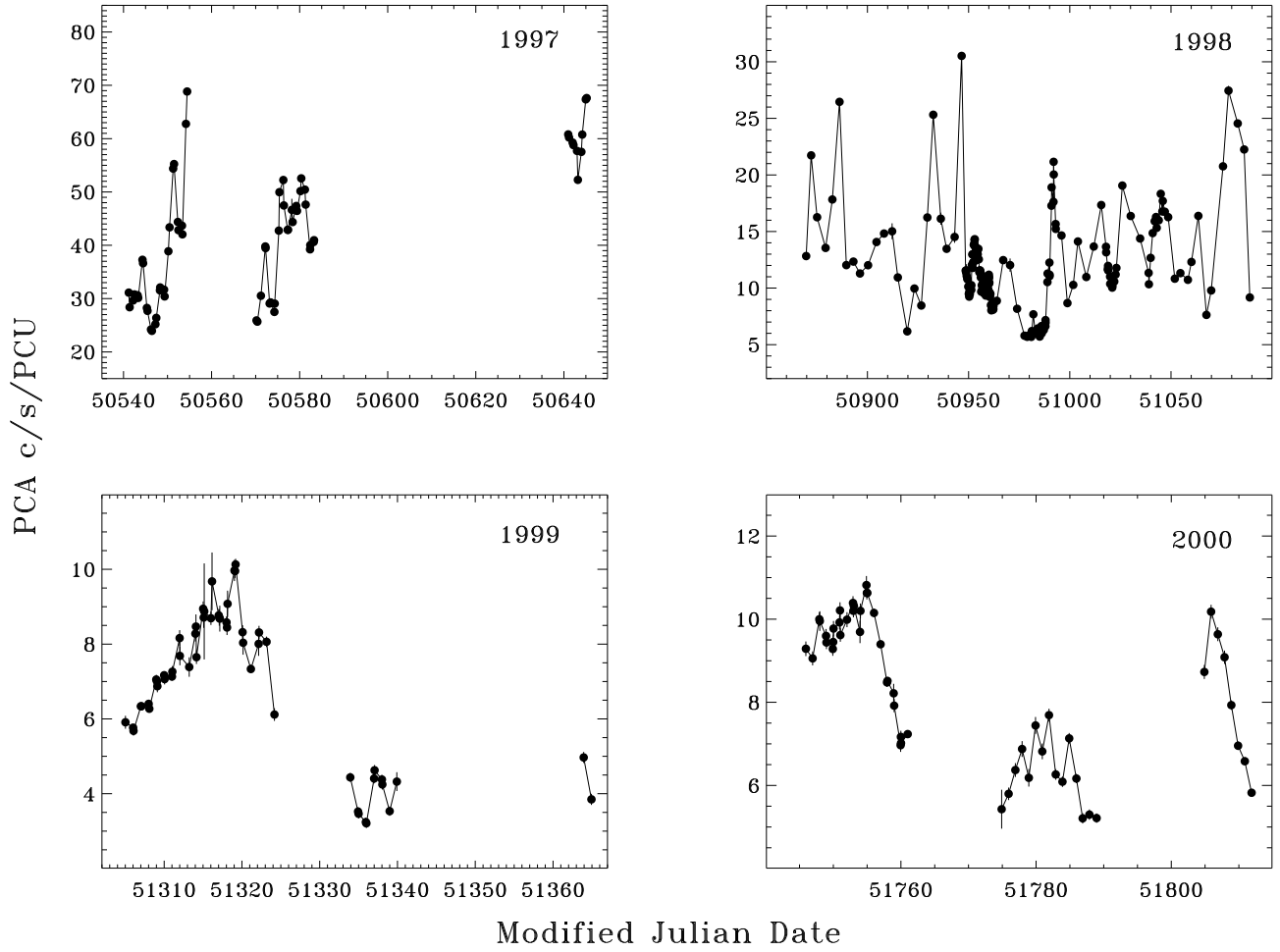


Fig. 4.— PCA light curves of Mrk 501. Unlike in Fig. 3, the results here were derived from the PCU 2 data alone. For clarify, they are shown for each year separately.

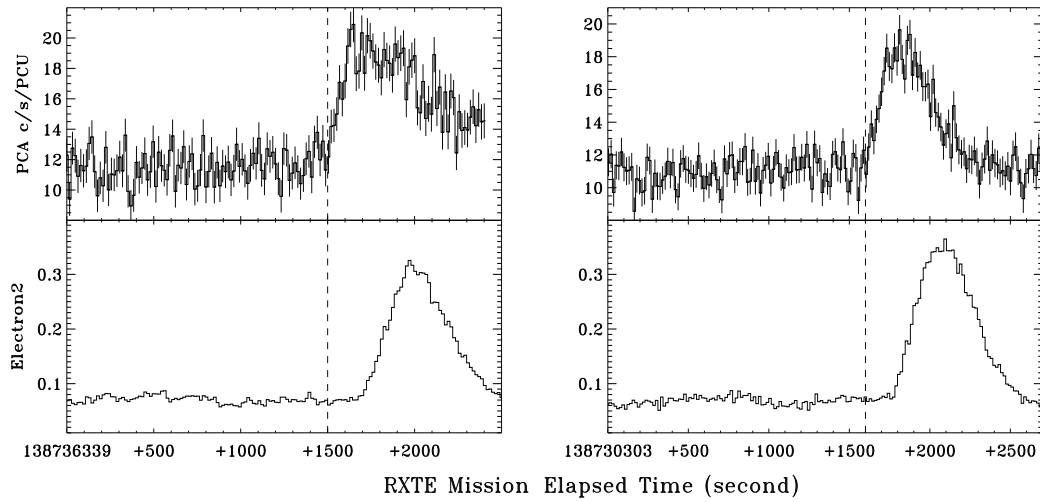


Fig. 5.— (left) Reported sub-hour X-ray flare (Catanese & Sambruna 2000). It is seen only after the data filtering criterion on the “ELECTRON2” parameter is relaxed. Note the 200-second lead of the X-ray flare with respect to the electron flare. (right) A similar X-ray flare, with almost identical 200-second difference between the starting time of the X-ray and electron flares. For reference, the RXTE Mission Elapsed Time (MET) is used, which is defined as the number of seconds since 1994 January 1 00:00:00 (UT).

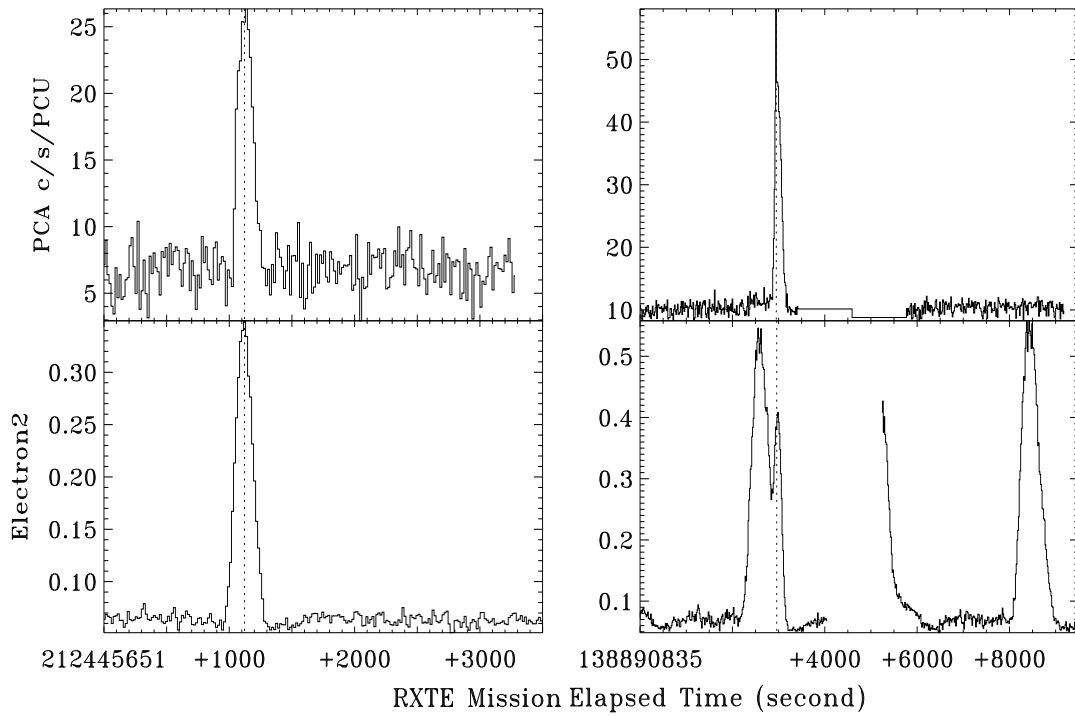


Fig. 6.— Sample X-ray flares with associated electron flares. Note that not all electron flares induce X-ray flares and that an electron flare may have a complicated multi-peaked profile.

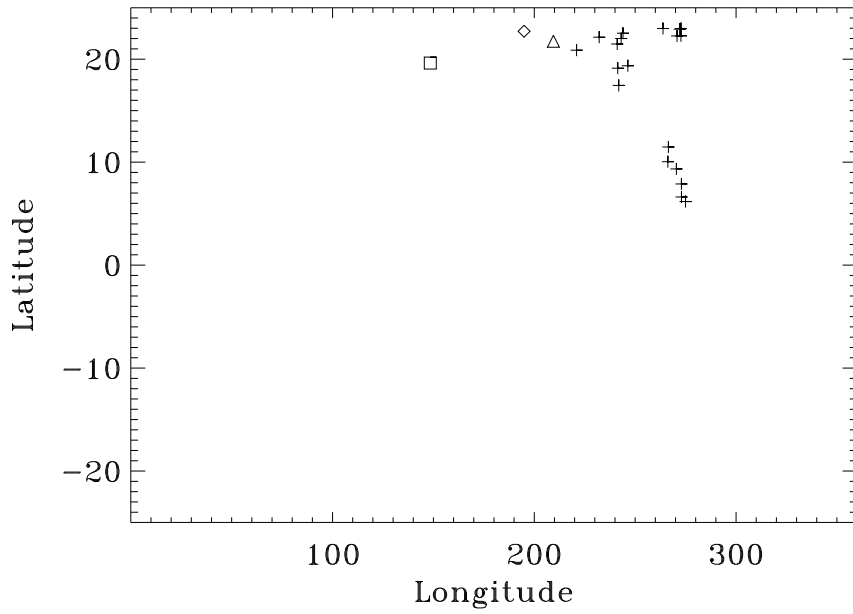


Fig. 7.— Satellite positions at the times of the peaks of electron flares. The two flares shown in Fig. 5 are indicated by different symbols, with the one associated with the reported X-ray flare in open diamond and the other in open triangle. Purely for the purpose of comparison, the X-ray flare shown in Fig. 8 is also indicated here (in open square). It should be stressed, however, that it is *not* accompanied by any electron flare; in this case, the satellite position was derived from the starting time of the X-ray flare.

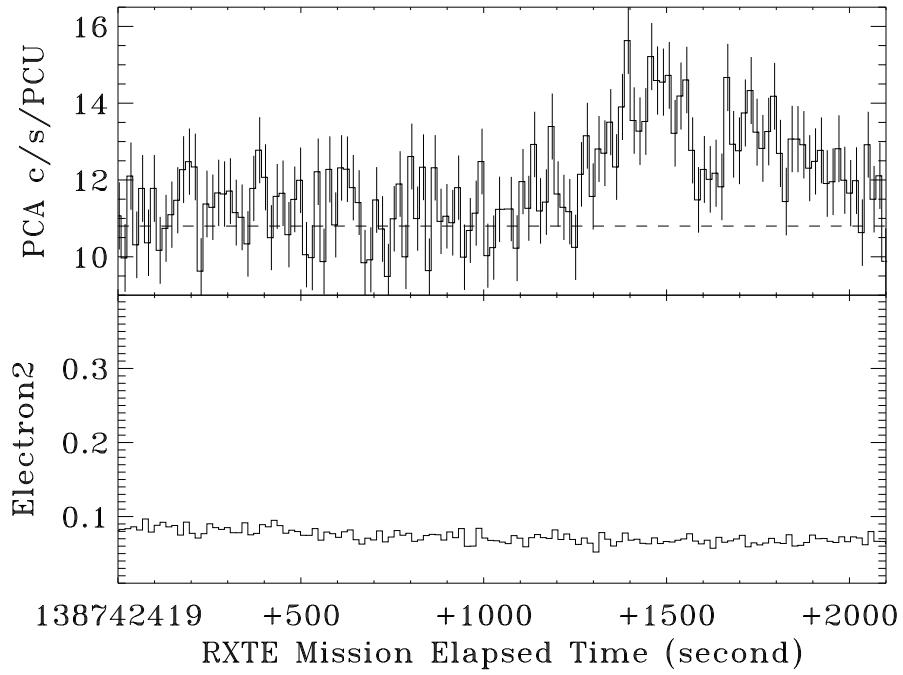


Fig. 8.— Same as Fig. 5 but for a real sub-hour X-ray flare from Mrk 501. Note sub-structures in the profile of the flare.

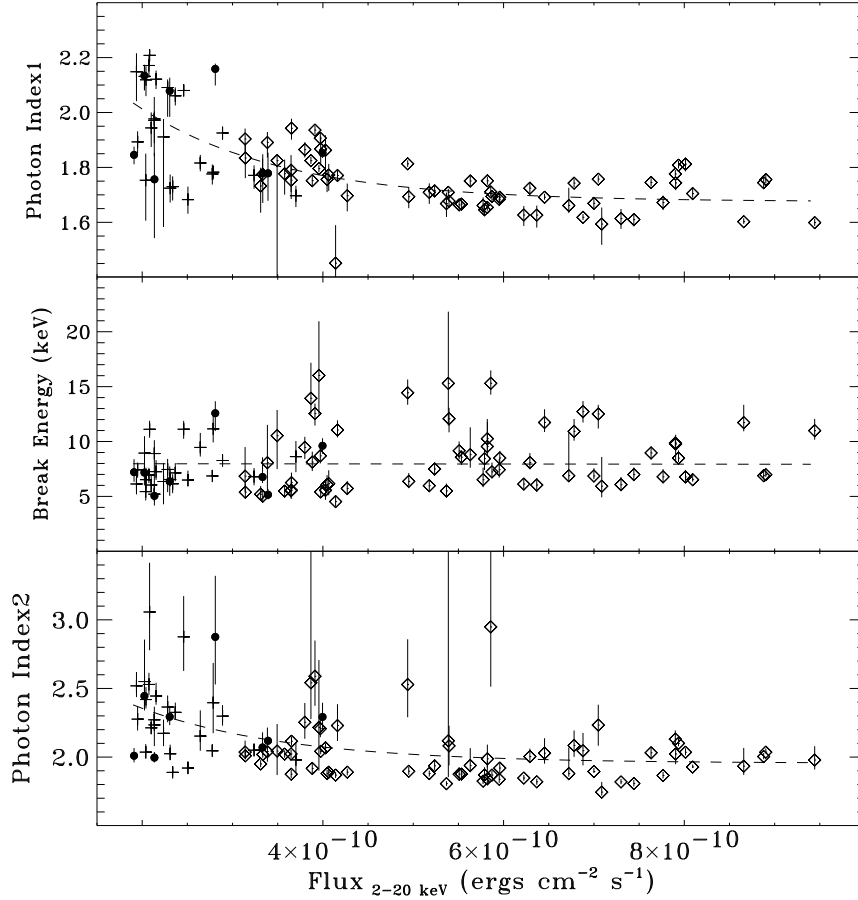


Fig. 9.— Flux dependence of the model parameters. The results were obtained with a broken power law and are shown in diamonds for observations taken in 1997, in filled circles for those (taken in 1998) near the end of the decaying phase of the 1997 giant flare, and in crosses for those during the rising phase of the 1998 flare (with the dividing line between the two 1998 period drawn somewhat arbitrarily at MJD 50960.6; see Fig. 1). To guide the eye, the dashed lines are drawn to show best-fits to the data with a model consisting of a constant plus an exponential function.

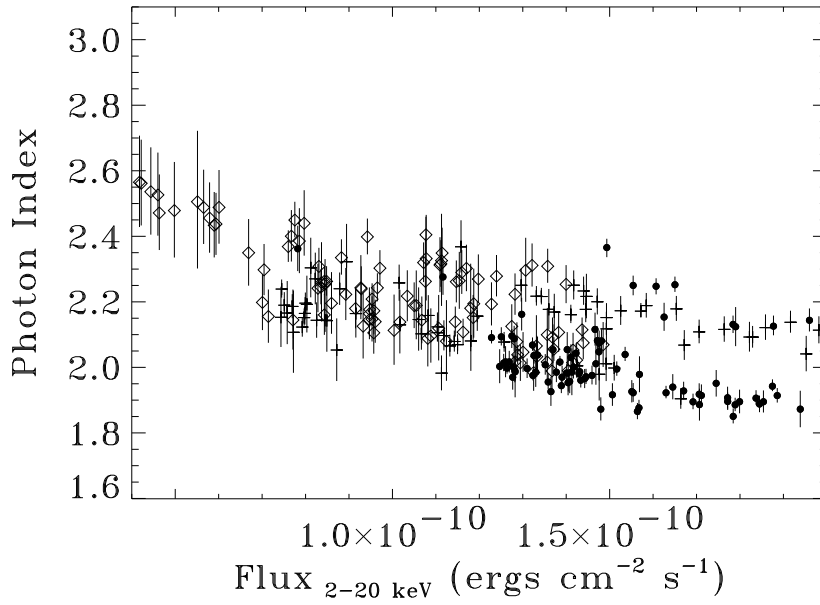


Fig. 10.— Same as Fig. 9, but a simple power law was used to fit the data. The results are shown in diamonds for observations taken in 1999 and 2000, in crosses for those during the rising phase of the 1998 flare, and in filled circles for those near the end of the decaying phase of the 1997 flare.

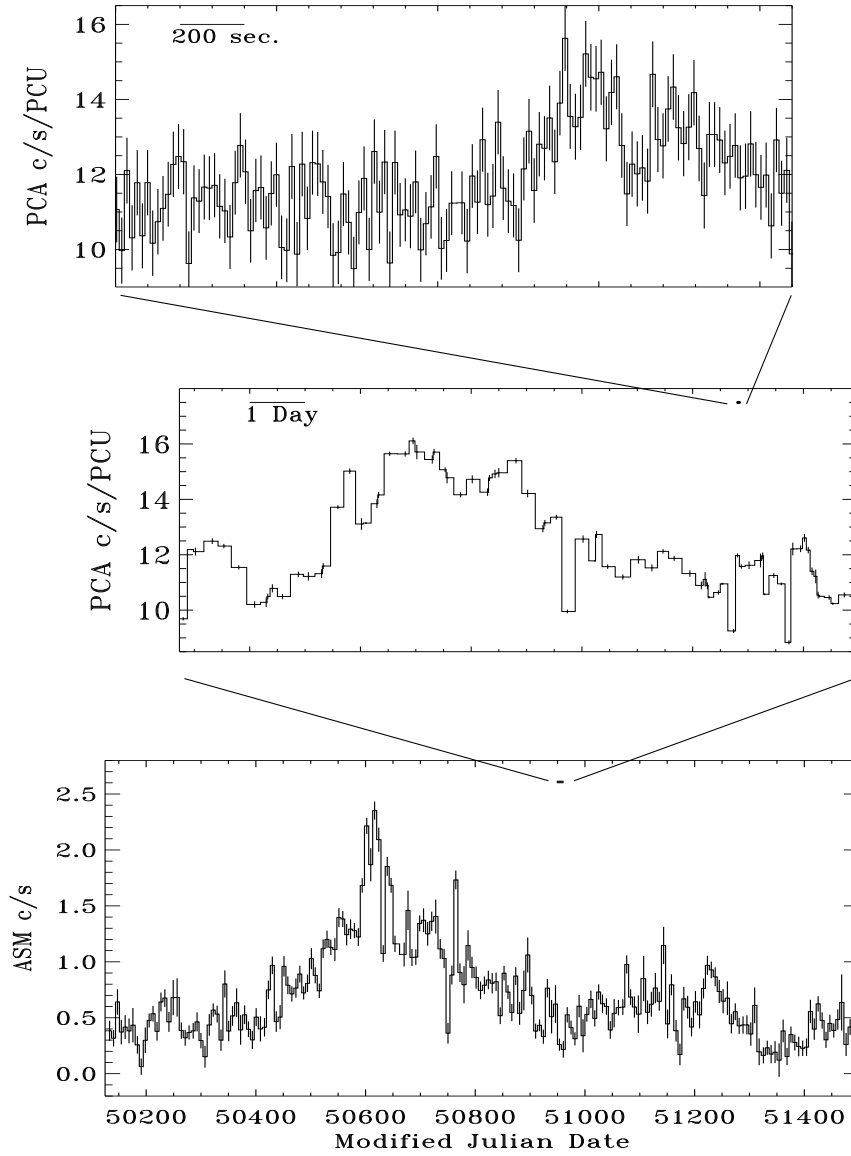


Fig. 11.— X-ray flares from Mrk 501 on a wide range of timescales. Apparent irregularity in the width of histogram bins is a manifestation of irregular data sampling.